

Detection of Atmospheric Neutrinos and Relativistic Nuclear Structure Effects

Hungchong Kim ^{*} ^{1,2}, S. Schramm [†] ³, C. J. Horowitz [‡] ¹

¹ *Nuclear Theory Center, Indiana University, Bloomington, Indiana 47408, USA*

² *Department of Physics, Yonsei University, Seoul, 120-749, Korea*

³ *GSI, D-64220 Darmstadt, Germany*

(July 29, 2021)

Abstract

Neutrino-nucleus cross sections for the detection of atmospheric neutrinos are calculated in relativistic impulse and random phase approximations. Pion production is estimated via inclusive Δ -hole nuclear excitations. The number of pion events can confuse the identification of the neutrino flavor. As a further source of pions we calculate coherent pion production (where the nucleus remains in the ground state). We examine how these nuclear structure effects influence atmospheric neutrino experiments and study possible improvements in the present detector simulations.

*E-mail: hung@phya.yonsei.ac.kr

†E-mail: schramm@tpri6e.gsi.de

‡E-mail: charlie@proteus.iucf.indiana.edu

I. INTRODUCTION

Aside from the puzzling solar neutrino data there exist extensive measurements of atmospheric neutrinos, which are produced in cosmic ray interactions with the earth's atmosphere. Cosmic rays, mostly protons or α particles, hitting the atmosphere produce pions, which undergo the following decays:

$$\begin{aligned}\pi^\pm &\rightarrow \mu^\pm + \nu_\mu (\bar{\nu}_\mu) \\ \mu^\pm &\rightarrow e^\pm + \nu_e (\bar{\nu}_e) + \bar{\nu}_\mu (\nu_\mu) .\end{aligned}$$

From this, one expects the neutrino flavor ratio,

$$r = \frac{\nu_\mu + \bar{\nu}_\mu}{\nu_e + \bar{\nu}_e} , \quad (1)$$

to be about 2. However, two existing experiments, IMB [1] and Kamiokande [2], consistently measured a ratio of about 1 by studying charged-current neutrino-nucleus reactions $[(\nu_e, e)$ and $(\nu_\mu, \mu)]$ in large underground water detectors. This could mean either there is a depletion of muon-type neutrinos or an enhancement of electron-type neutrinos. While the separate ν_μ and ν_e neutrino fluxes differ in various calculations, their ratio, however, seems to be largely model-independent [3], and the theoretical results are in clear contradiction with data. This discrepancy is known as the ‘‘atmospheric neutrino anomaly’’.

One explanation of this result could be the existence of neutrino oscillations of the muon neutrino into some other neutrino species [4] which would reduce the ν_μ flux. However, before drawing this conclusion, one should also investigate more conventional sources for uncertainties in the measured flux ratio, which originate from nuclear physics and detector specifics. One crucial point is the experimental separation of electron and muon events. Most data are measured using water detectors. In a charged-current weak interaction with an ^{16}O nucleus, the incoming neutrino generates an outgoing lepton which is detected through its Čerenkov radiation. Electrons and muons are distinguished by the characteristics of their tracks. Electrons produce a showering ‘‘fuzzy’’ track, whereas muons are identified by their nonshowering track.

Pions constitute a major background in this way of determining the neutrino flavors. In the experimental analysis, two- and more ring events, which signal the production of several charged particles, are rejected. However, a charged pion can be confused with a muon event if the lepton energy is below Čerenkov radiation threshold, and a neutral pion, with one decay photon missing, can be counted as an electron event. Therefore, a reasonable determination of the flavor ratio can only be achieved when the pion events are properly taken into account.

One major source of pions is the decay of a Δ produced in the neutrino scattering. The delta can subsequently decay into a pion and a nucleon. An estimate of the number of pion events is only possible when the Δ -h response is properly calculated. Indeed, Monte Carlo simulation of the Kamiokande experiment [5] estimated the number of pion events based on a rather complicated nonrelativistic model [6]. However, atmospheric neutrinos have a broad energy spectrum ranging from a few hundred MeV to several GeV. It is therefore crucial to have a relativistic formalism that allows the calculation of the cross section for arbitrary kinematics.

As another source of pions, we consider coherent pion production and its role in the detection of atmospheric neutrinos. Coherent pions are produced in both charged- and neutral-current neutrino-nucleus interactions which leave the nucleus in its ground state. Traditionally, the coherent π^0 's are distinguished from the resonantly produced pions due to their strongly forward peaked angular distribution. However, in atmospheric neutrino experiments, due to a lack of directional information of the incoming neutrinos, it is not possible to distinguish the coherent π^0 events from incoherent pions.

In the case of coherent charged pions the forward angle dominance of the cross section leads to a small opening angle between two charged particles (μ or e and charged pion) in the final state, and these two particles could be detected as one isolated electromagnetic shower. In contrast to incoherent charged pions whose Čerenkov tracks are usually identified as muon events, the special characteristics of coherent pions could lead to an increase of identified ν_e events and thus to underestimating the ν_μ to ν_e ratio.

This paper is organized as follows. In Sec. II we present the formalism for neutrino-nucleus cross section including p-h and Δ -h nuclear excitations within the framework of a relativistic mean-field model of the nucleus. Sec. III contains the formalism for coherent charged and neutral pion production. The resulting cross sections and production rates are shown in Sec. IV. We close with a discussion and outlook in Sec. V.

II. INCLUSIVE CROSS SECTION

We outline the formalism for inclusive neutrino-nucleus scattering cross section including p-h (nucleon particle-hole) and Δ -h (delta-hole) nuclear excitations. We consider a neutrino with four-momentum $k = (E_\nu, \mathbf{k})$ which scatters from a nucleus via W^\pm boson exchange producing a charged lepton with four-momentum $k' = (E_{\mathbf{k}'}, \mathbf{k}')$. Using impulse approximation, the double differential scattering cross section from a target nucleus with mass number A is given by (we assume a symmetric $N = Z$ nucleus):

$$\frac{d^2\sigma}{d\Omega_{\mathbf{k}'} dE_{\mathbf{k}'}} = -\frac{AG_F^2 \cos^2\theta_c |\mathbf{k}'|}{32\pi^3 \rho E_\nu} \text{Im} [L_{\mu\nu} \Pi_A^{\mu\nu}] . \quad (2)$$

Here $\rho = 2k_F^3/3\pi^2$ is the baryon density with Fermi momentum k_F , θ_c the Cabbibo angle ($\cos^2\theta_c = 0.95$), G_F is the Fermi constant. The leptonic tensor $L_{\mu\nu}$ is defined as

$$L_{\mu\nu} = 8 \left(k_\mu k'_\nu + k_\nu k'_\mu - k \cdot k' g_{\mu\nu} \mp i\epsilon_{\alpha\beta\mu\nu} k^\alpha k'^\beta \right) , \quad (3)$$

with the minus (plus) sign denoting neutrino (anti-neutrino) scattering. $\Pi_A^{\mu\nu}$ is the polarization tensor of the target nucleus for the charged weak current. Here we consider p-h, $\Pi_{ph}^{\mu\nu}$, and Δ -h, $\Pi_{\Delta h}^{\mu\nu}$, contributions to the polarization:

$$\Pi_A^{\mu\nu} = \Pi_{ph}^{\mu\nu} + \Pi_{\Delta h}^{\mu\nu} . \quad (4)$$

In the impulse approximation, the p-h polarization takes a simple form,

$$i\Pi_{ph}^{\mu\nu} = \int \frac{d^4p}{(2\pi)^4} \text{Tr}[G(p+q) \Gamma^\mu G(p) \Gamma^\nu] , \quad (5)$$

with the weak-interaction vertex given in terms of single-nucleon form factors parameterized from on-shell data,

$$\Gamma^\mu(q^2) = F_1(q^2)\gamma^\mu + iF_2(q^2)\sigma^{\mu\nu}\frac{q_\nu}{2M} - G_A(q^2)\gamma^\mu\gamma^5 + F_p(q^2)q^\mu\gamma^5, \quad (6)$$

$$(q^2 \equiv q_0^2 - \mathbf{q}^2)$$

The form factors F_1, F_2, G_A and F_p are given in the appendix of Ref. [7]. The pseudoscalar form factor F_p is constructed from PCAC, and its contribution is suppressed by the small lepton mass.

In an approximation where the nucleus is in a mean-field ground state of the Walecka model, the nucleon propagator $G(p)$ is given by [8]

$$G^*(p) = (\not{p}^* + M^*) \left[\frac{1}{p^{*2} - M^{*2} + i\epsilon} + \frac{i\pi}{E_{\mathbf{p}}^*} \delta(p_0^* - E_{\mathbf{p}}^*) \theta(k_F - |\mathbf{p}|) \right], \quad (7)$$

where the effective mass M^* and energy $E_{\mathbf{p}}^*$ are shifted from their free-space value by the scalar (S) and timelike component (V) of the mean fields,

$$M^* = M + S; \quad E_{\mathbf{p}}^* = \sqrt{\mathbf{p}^2 + M^{*2}}; \quad p^{*\mu} = (p^0 - V, \mathbf{p}). \quad (8)$$

In the Fermi gas approximation of non-interacting particles, V and S are set to zero. Analytic expressions for the imaginary part of the polarization [Eq. (5)] can be found in Ref. [7].

The impulse approximation can be improved by including RPA effects. An RPA calculation uses the same expression for the cross section as in Eq. (2) with the replacement:

$$\Pi^{\mu\nu} \rightarrow \Pi_{RPA}^{\mu\nu} = \Pi^{\mu\nu} + \Delta\Pi_{RPA}^{\mu\nu}. \quad (9)$$

$\Delta\Pi_{RPA}^{\mu\nu}$ represents many-body correlations mediated by isovector particles, π and ρ incorporated with the Landau-Migdal parameter g' .

The cross section involving Δ -h excitations is calculated similarly in Hartree approximation [9] using the Δ -h polarization $\Pi_{\Delta h}^{\mu\nu}$. The weak interaction contains vector current (v) and axial-vector current (a) contributions, therefore, we split $\Pi_{\Delta h}^{\mu\nu}$ into

$$\Pi_{\Delta h}^{\mu\nu} = (\Pi_{\Delta h}^{vv})^{\mu\nu} + (\Pi_{\Delta h}^{aa})^{\mu\nu} + (\Pi_{\Delta h}^{va})^{\mu\nu} + (\Pi_{\Delta h}^{av})^{\mu\nu}. \quad (10)$$

Here $(\Pi_{\Delta h}^{va})^{\mu\nu}$ and $(\Pi_{\Delta h}^{av})^{\mu\nu}$ are interference terms of the vector and axial-vector currents. These polarization tensors are written in terms of the spin 3/2 delta propagator and appropriate weak vertices as,

$$\begin{aligned} (\Pi_{\Delta h}^{ij})_{\mu\nu} = & -i \int \frac{d^4 p}{(2\pi)^4} \text{Tr}[\Gamma_{\beta\mu}^i(-q, -p) S^{\beta\alpha}(p) \Gamma_{\alpha\nu}^j(q, p) G(p - q)] \\ & + (q_\mu \rightarrow -q_\mu) \quad (i, j) = (a, v). \end{aligned} \quad (11)$$

The trace is taken for the Dirac matrices as well as the isospin matrices. For $S^{\mu\nu}(t)$ we take the Rarita-Schwinger form of the free spin 3/2 propagator with momentum t :

$$S^{\mu\nu}(t) = -\frac{\not{t} + M_\Delta}{t^2 - M_\Delta^2 + i\epsilon} \left[g^{\mu\nu} - \frac{1}{3}\gamma^\mu\gamma^\nu - \frac{2}{3}\frac{t^\mu t^\nu}{M_\Delta^2} + \frac{t^\mu\gamma^\nu - t^\nu\gamma^\mu}{3M_\Delta} \right]. \quad (12)$$

The vector part of the nucleon-delta vertex has been studied in the case of the $\gamma N\Delta$ transition [10],

$$\begin{aligned}\Gamma_{\mu\nu}^V(q, p) &= \sqrt{2}F^\Delta(Q^2)T^\pm \left[(-q_\mu\gamma_\nu + g_{\mu\nu} \not{q})M_\Delta\gamma_5 + (q_\mu p_\nu - q \cdot p g_{\mu\nu})\gamma_5 \right] \\ &\equiv \sqrt{2}F^\Delta T^\pm V_{\mu\nu}\end{aligned}\quad (13)$$

with the isospin raising or lowering operator T^\pm [9]. The vertex for the axial $N\Delta$ transition is given by [11–13]

$$\Gamma_{\mu\nu}^A = -\frac{r_{N\Delta}}{\sqrt{2}}G_A T^\pm (g_{\mu\nu} - \frac{\gamma_\mu\gamma_\nu}{4}) \quad (14)$$

with $r_{N\Delta} = f_{\pi N\Delta}/f_{\pi NN} \sim 2$. The form factors F^Δ and G_A are defined in the appendix of Ref. [9].

In mean-field approximation, the propagation of a Δ is modified by background scalar and vector fields similarly as the nucleon propagator. This can be understood from a chiral soliton model where the delta is a rotational excitation of the nucleon. That is, in the medium, the delta is expected to be influenced by the same magnitude of the vector and scalar potentials as the nucleon's because σ and ω are isoscalar. The calculation of the cross section proceeds in the same way as in the case of the free Δ .

To include the delta decay width in our calculation, we average the nuclear response over the delta mass with a Breit-Wigner distribution [10]. The averaged cross section follows as

$$\langle \frac{d^2\sigma}{d\Omega_{\mathbf{k}'}dE_{\mathbf{k}'}} \rangle \sim \int d\mu^2 \frac{d^2\sigma}{d\Omega_{\mathbf{k}'}dE_{\mathbf{k}'}}(\mu) f(\mu^2) / \int d\mu^2 f(\mu^2) \quad , \quad (15)$$

$$f(\mu^2) = \frac{M_\Delta\Gamma_\Delta}{(M_\Delta^2 - \mu^2)^2 + M_\Delta^2\Gamma_\Delta^2} \quad (16)$$

integrating from threshold to infinity. However, the decay width of a delta in the nuclear medium is not well determined both theoretically and experimentally. The πN decay channel of the delta is partially blocked by Pauli blocking but there is an additional spreading width. Thus, determining the in-medium decay width is a nontrivial problem. Here, we assume the in-medium width to be the same as the free width $\Gamma_\Delta = 115$ MeV. More theoretical and experimental work has to be done regarding this question, however.

III. COHERENT PION PRODUCTION

Coherent pions are produced as decay products of virtual p-h or Δ -h excitations of a finite nucleus. More specifically, the momentum transfer from the incoming neutrino virtually excites the nucleus through p-h or Δ -h and the nucleus decays back to its ground state by emitting a pion. Here we derive the formalism for the Δ -h excitation as it dominates the p-h excitations of the nucleus. The corresponding scattering diagram is shown in Fig. 1. Note that the coherent pion is on-shell even though the momentum transfer in the initial scattering is space-like. The missing momentum is provided by the recoil of the nucleus.

In a local density approximation, the finite-nucleus polarization $\Pi_{\text{FN}}(q, q'; \omega)$ with incoming and outgoing momenta q and q' , respectively, is approximated in terms of the nuclear matter polarization $\Pi_{\text{NM}}(q, q'; \omega)$,

$$\Pi_{\text{FN}}^\mu(q, q'; \omega) = V F(|\mathbf{q} - \mathbf{q}'|) \Pi_{\text{NM}}^\mu(q, q'; \omega) , \quad (17)$$

where $F(|\mathbf{q} - \mathbf{q}'|)$ is the elastic form factor of the target nucleus. We obtain $F(|\mathbf{q} - \mathbf{q}'|)$ by Fourier transforming the nuclear ground state density obtained from a self-consistent relativistic mean field calculation for finite nuclei [14]. The volume for a target nucleus with mass number A is given by

$$V = \frac{3\pi^2 A}{2k_F^3} .$$

As shown in Fig. 1, the incoming neutrino interacts weakly with the nucleus exciting an intermediate Δ -h state. The vertex of the weak interaction contains vector and axial-vector parts while the $\pi N \Delta$ vertex, on the other hand, involves only the axial-vector part contracted with a pion four-momentum q' . Since the coherent-pion production cross section is dominated by pion momenta \mathbf{q}' parallel to the momentum transfer \mathbf{q} , there is negligible contribution from the part of the polarization that mixes the axial-vector and vector current. We ignore this small contribution throughout this paper. Consequently, the cross section for coherent pion production is identical for neutrinos and antineutrinos.

The double differential cross section for coherent pion production is

$$\begin{aligned} \frac{d^2\sigma}{dE_\pi d\Omega_{\mathbf{k}'}} &= \frac{|\mathbf{k}'||\mathbf{q}'| G_F^2 V^2}{256\pi^4 E_\nu} \int_{-1}^1 d\cos\theta_{q'} F^2(\cos\theta_{q'}) \left[L_{00} |\Pi_{\text{NM}}^0|^2 \right. \\ &\quad \left. + 2L_{01} \text{Re}[\Pi_{\text{NM}}^0 (\Pi_{\text{NM}}^1)^*] + L_{11} |\Pi_{\text{NM}}^1|^2 \right] , \end{aligned} \quad (18)$$

where $\theta_{q'}$ is the angle between \mathbf{q} and \mathbf{q}' . Here we observed that the integral in Eq. (18) is dominated by small angles, which implies that contributions from transverse components of the polarization, Π_{NM}^2 and Π_{NM}^3 , are suppressed. Energy conservation requires the pion energy E_π to be equal to the energy transfer to the nucleus q_0 . The pion three-momentum \mathbf{q}' is obtained from the mass-shell condition

$$|\mathbf{q}'| = \sqrt{q_0^2 - m_\pi^2} . \quad (19)$$

The antisymmetric part of the leptonic tensor $L_{\mu\nu}$ does not contribute to Eq. (18), as it is contracted with the vector axial-vector mixing term of the polarization. The nuclear matter polarization, Π_{NM}^μ , can be evaluated for coherent charged or neutral pion production by taking appropriate vertices. The calculation of the real and imaginary parts of the polarizations Π_{NM}^0 and Π_{NM}^1 is summarized in Appendix.

In a relativistic mean field approximation, the properties of the nucleon and Δ are modified by strong scalar and vector fields in the nuclear medium. These effects can be incorporated by modifying the nucleon and delta propagators as we described in the inclusive calculation. Since the axial-vector vertex does not contain the energy of the Δ or nucleon, the contribution from the constant vector mean-fields is eliminated in the calculation of the polarization by a simple change of integration variable. As the Δ is unstable, we include a width Γ_Δ by using a complex mass M_Δ^c

$$M_\Delta \rightarrow M_\Delta^c \equiv M_\Delta - i \Gamma_\Delta / 2 , \quad (20)$$

in the denominator of the delta propagator [11]. This prescription yields similar results as the usual Breit-Wigner folding. Note, we have not included pion distortions in Eq. (18). These may somewhat reduce the cross section. The effect of distortions and a possible Δ -h spreading potential remain to be investigated.

IV. RESULTS

In this section, we present numerical results of our calculation. We start with the inclusive cross sections and their role in atmospheric neutrinos followed by a discussion of the coherent pions. In the case of the inclusive cross section, we discuss the case of muon neutrinos, but the general features of the results hold for electron neutrinos as well. In addition to the relativistic Fermi gas description of the nucleus, the effects of mesonic mean fields are also considered in the mean-field approximation (MFA). The target nucleus is assumed to be ^{16}O with a Fermi momentum $k_F = 225$ MeV. In MFA, we use the same scalar and vector couplings for nucleon and delta (“universal coupling”). For $k_F = 225$ MeV, the effective masses are

$$M_{\Delta}^* = 931\text{MeV} ; \quad M_N^* = 638\text{MeV} , \quad (21)$$

and the vector self-energy is $V = 239$ MeV.

In atmospheric neutrino experiments such as Kamiokande and IMB [1,2], the cross section of interest is $d\sigma/dE_{\mathbf{k}'}$, which is obtained from Eq. (2) by another numerical integration over the scattering angle of the outgoing lepton. Fig. 2 shows the cross section $d\sigma/dE_{\mathbf{k}'}$ for $E_{\nu} = 1$ GeV. Note that the cross sections from the p-h excitation are peaked at a large lepton energy, which corresponds to a small nuclear excitation energy. This is the region where nucleon correlations are important. The nucleon correlations are modeled using RPA which includes a $(\rho + \pi + g')$ residual isovector interaction. The RPA calculation¹ in the mean-field ground state is also shown in Fig. 2. The cross section for stable deltas vanishes around $E_{\mathbf{k}'} = 0.7$ MeV, which gives the minimum energy transfer for delta production. The curves including the delta width, however, spread over to higher lepton energies because of the averaging process.

The mean fields reduce the p-h and the Δ -h responses by 30% at the peaks. However, RPA effects reduce the peak by 50% at high muon energies. The reduction of the Δ -h response by mean fields is interesting in the Monte Carlo simulation of atmospheric neutrino experiments. The strength of the Δ -h cross section provides the number of pions produced from the Δ decays. These pions may cause an uncertainty in determining the lepton flavor in the experiment. Indeed, the Monte Carlo simulation of the Kamiokande detector [5] takes into account the number of pion events based on a nonrelativistic model by Fogli and Nardulli [6]. Their nonrelativistic results are qualitatively reproduced in our free delta calculations. Thus mean-field effects are not included in the existing simulations and could provide significant systematic errors.

To get a rough estimate of the reduction in the number of events, we fold $d\sigma/dE_{\mathbf{k}'}$ with a simple model of the atmospheric neutrino flux. We approximately fit the atmospheric muon neutrino flux with the formula [2]

$$\phi_{\nu_{\mu}}(E_{\nu}) = 220 E_{\nu}^{-2.5} \frac{1}{\text{m}^2 \text{ sr GeV sec}} , \quad (22)$$

and assume

¹Note that our RPA calculations do not include Δ -h or mixtures of p-h and Δ -h.

$$\phi_{\bar{\nu}_\mu} = \phi_{\nu_\mu} = 2\phi_{\nu_e} = 2\phi_{\bar{\nu}_e} . \quad (23)$$

Using this flux, we calculate the yield Y in units of events per Kton year of detector exposure and per 100 MeV energy bin,

$$Y = 1.1938 \times 10^{40} \int \phi_{\nu_\mu}(E_{\nu_\mu}) \frac{d\sigma}{dE_{\mathbf{k}'}} dE_{\nu_\mu} , \quad (24)$$

and plot the result in Fig. 3 (a) with respect to the muon energy for the p-h and Δ -h excitations. Note, the Δ -h calculations include the decay width of the delta of 115 MeV. However, in the case of the inclusive process the quantitative results are insensitive to the decay width. At low muon energies, the mean fields in the impulse approximation reduce the total p-h events from 33 to 28 while including RPA yields 22 events (in a 100 MeV bin after one Kton Year of exposure assuming 100 percent efficiency). Thus, nuclear structure effects reduce the quasielastic charged-current events substantially. Since the electron events are also reduced by a similar amount by RPA correlations, this reduction does not directly affect the ratio r of Eq. (1). However, it can change the *energy dependence* of the cross section.

Also, as one can see from Fig. 3 (b), the Δ -h contribution is about 40% of the RPA calculation at its minimum and, as the muon energy increases, the Δ -h response becomes more important. The Δ -h response is even larger than the RPA response at high muon energies (the ratio is 1.06 at $E_{\mathbf{k}'} = 2$ GeV). Note that the Δ -h response is reduced by 10% to 25% due to mean-fields. Incoherent pion events should be decreased correspondingly. Therefore, the reduction due to the Δ mean-fields combined with the event reduction from RPA should be properly taken into account in the simulation.

Not all deltas decay to πN in the nuclear medium. In fact, in the medium the πN decay is partially suppressed because of Pauli blocking [15]. However, the Δ in the medium has additional channels of pionless decay. The coincidence experiments of (p, n) reactions at the Δ resonance [16] showed that a large portion of deltas in the medium decay without emitting pions. Furthermore, in theoretical calculations, a value of about 70 MeV has been used as the 2p-2h partial width [18,17]. Thus, experimental and theoretical results indicate a substantial amount of pionless delta decay in the medium. This 2p-2h decay mode of the delta has not been directly included in present detector simulations. At best, its effects have been partially incorporated using a very crude model of pion absorption without any explicit reference to Δ production.

The pionless decay of the delta and the reduction due to the mean-fields, suggest that the simulations may substantially overcount the total number of pions. At this moment, we do not know how these effects change the result for the atmospheric neutrino anomaly. But the results indicate that the Monte Carlo simulations in current atmospheric neutrino experiments can be improved to treat pion events more accurately.

Now we present results for coherent pion production in neutrino scattering. Coherent pions may be important in atmospheric neutrino experiments because they could increase the electron-like events and therefore reduce the ratio r of Eq. (1). A coherent neutral pion produced in neutral-current scattering (ν, ν') immediately decays into two photons and may be counted as an electron-like event. Likewise, a coherent charged pion can also be confused with an electron-like event when the two charged particles in the final state,

muon (or electron) and charged pion, move with small opening angle and make an isolated electromagnetic shower. Indeed small-angle scattering dominates the coherent cross section.

The single differential cross section $d\sigma/dE_\pi$ is obtained by numerically integrating Eq. (18) over the scattering solid angle. Again, we use the free width $\Gamma_\Delta = 115$ MeV in our calculation. Pauli-blocking and additional decay channels for the Δ in the medium will change this value (and generate a non-trivial momentum-dependence). However, as theoretical in-medium values are still very uncertain, we will not explore modifications of the width at this point. More work in this direction has to be done in the future.

In the atmospheric neutrino experiments, both μ - and e -neutrinos participate in producing coherent pions. Furthermore, in contrast to the inclusive scattering process where the cross sections of antineutrinos are strongly suppressed, neutrino and antineutrino contributions to coherent pion production are of the same size. Combining the events from μ -type antineutrinos as well as e -type neutrinos and antineutrinos could enhance coherent pion production substantially, and it is of interest to quantitatively compare the coherent pion events directly with the inclusive charged-current events through p-h nuclear excitation for a realistic spectrum of neutrinos.

Using the e -neutrino flux ($\phi_{\nu_e} = \phi_{\bar{\nu}_e}$), we calculate the coherent pion events and compare them with electron production in ν_e scattering. The neutral pion events per kiloton-year are

$$Y(\pi^0) = 6 \times 1.194 \times 10^{40} \int \phi(E_{\nu_e}) \frac{d\sigma}{dE_\pi}(E_{\nu_e}) dE_{\nu_e} . \quad (25)$$

The factor 6 includes the contribution from antineutrinos as well as a factor of 2 from μ -neutrinos. Note, for the purposes of illustration, let us assume all coherent pion events result in electron-like tracks. The actual identification of these events depends on the details of a detector. Fig. 4 (a) shows the coherent π^0 events with and without mean fields and Δ decay width. The electron events from are obtained from

$$Y(e) = 1.194 \times 10^{40} \int \phi(E_{\nu_e}) \frac{d\sigma}{dE_{\mathbf{k}'}}(E_{\nu_e}) dE_{\nu_e} . \quad (26)$$

The differential cross section $d\sigma/dE_{\mathbf{k}'}$ is calculated in relativistic impulse and in random phase approximation [7]. Note that the horizontal axis in Fig. 4 (a) shows either the coherent pion or the electron energy.

Figure 4 (a) also shows that at roughly $E = 300$ MeV the coherent pion events, neglecting decay width and mean fields, are comparable in size to electron events calculated in RPA. This is certainly interesting because the electron-like events can be increased by these pions and therefore might help to explain the small ratio r of atmospheric neutrinos at $E = 300$ MeV. However, inclusion of mean fields reduces the pion events by a factor of 2. Furthermore, the Δ decay width exacerbates the situation: the number of events including mean fields and Δ decay width (thin dashed line) are only 10% of the electron events calculated in RPA.

Next, we consider the coherent charged pion events. In this case, the Čerenkov light detector records the total energy of pion and muon (or electron) assuming they are moving with small opening angle and make an isolated single track. Overall energy conservation implies

$$E_{\nu_\mu} = E_\pi + E_\mu \quad \text{or} \quad E_{\nu_e} = E_\pi + E_e \quad (27)$$

depending on the incoming neutrino type.

The coherent charged pion events are calculated from

$$\begin{aligned}
Y(\pi^\pm) = & 2 \times 1.194 \times 10^{40} \phi(E_{\nu_e}) \int_{m_\pi}^{E_\nu - m_e} \frac{d\sigma}{dE_\pi} dE_\pi \\
& + 4 \times 1.194 \times 10^{40} \phi(E_{\nu_e}) \int_{m_\pi}^{E_\nu - m_\mu} \frac{d\sigma}{dE_\pi} dE_\pi .
\end{aligned} \tag{28}$$

The first term results from e -neutrinos (the factor of 2 includes contribution from antineutrinos) and the second term originates from muon-type neutrinos (with a total flux factor of 4).

Figure 4 (b) shows the coherent charged pion events and the electron events calculated in RPA. As in the case of π^0 s neglecting mean field and decay width of the Δ results in cross sections for the coherent pions comparable or even larger than the quasielastic ones. However, again mean fields and the decay width substantially reduce the pion events: At $E = 1$ GeV, the full calculation amounts to only 23% of the quasielastic electron events, but at $E = 2$ GeV, it increases to 30%. Since the pion events become important as E increases, our findings provide an important systematic error to the interpretation of the recent Kamiokande experiment in the multi-GeV energy range [19].

The effect of neutral and charged coherent pions can be substantial, the actual numbers are very sensitive to the delta decay width, though. Coherent π^0 production could be large at $E = 300$ MeV while coherent charged pions may become important for high visible energies. To solidify our results, however, a more elaborate study of the Δ properties in the nucleus has to be performed.

V. SUMMARY

In this work, we have calculated neutrino-nucleus cross sections using a relativistic formalism to investigate possible improvements for the Monte Carlo simulation of Kamiokande experiment. We have found that RPA corrections reduce the charged-current neutrino events by up to 37% for particle-hole excitations. Because of this reduction, the Δ -h response could be important and is found to give significant corrections to quasi-elastic nucleon knock-out processes. We have found that the relativistic mean-fields reduce the Δ -h responses by 10% to 24%, which correspondingly reduce the pion events in atmospheric neutrino experiments. Combined with the additional channel of the non-pionic decay of the delta in the medium, our findings suggest possible uncertainties in the present Monte Carlo simulations of detectors and the interpretation of the measured data.

We have also discussed coherent pion production in neutrino-nucleus scattering. We have shown that coherent pions can produce a sizeable background in the atmospheric neutrino measurements. As neutral pions and collinearly outgoing charged leptons and pions may mimic electron-type events in the detector, this effect can produce uncertainties in determining the flavor ratio of the incoming neutrinos. Coherent pions may provide important systematic errors for the recent Kamiokande experiment in the multi-GeV energy region [19]. In order to get a clearer quantitative estimate of the influence of coherent pions, improved calculations should be done and these should be included in detector simulations of atmospheric neutrino experiments

ACKNOWLEDGMENTS

This research was supported in part by the DOE under Grant No. DE-FG02-87ER-40365 and the NSF under Grant No. NSF-PHY91-08036. The work of Hunchong Kim was also supported in part by the Basic Science Research Institute program of the Korean Ministry of Education through grant no. BSRI-95-2425.

APPENDIX:

Here we evaluate the nuclear matter polarization, $(\Pi_{\text{NM}})_\mu$, for coherent pion production. The polarization is defined as

$$\begin{aligned} (\Pi_{\text{NM}}^j)_\mu &= -i \int \frac{d^4 p}{(2\pi)^4} \text{Tr} \left[\Gamma_{\mu\beta}^j S^{\beta\alpha}(p') \Gamma_\alpha^j(q') G^o(p) \right] + (q_\alpha \rightarrow -q_\alpha) \\ &\equiv \Pi_{\mu\nu}^j(q) q'^\nu ; \quad j = (\pi^\pm, \pi^0), \end{aligned} \quad (\text{A1})$$

where $p' = p + q$. The superscript j indicates the polarization for the charged or neutral pion production. The axial-vector ($\Gamma_{\mu\nu}^j$) and pion (Γ_ν^j) vertices can be found from Ref. [11–13]. The noninteracting nucleon propagator in Hartree approximation reads

$$G^o(p) = (\not{p} + M) \frac{i\pi}{E_{\mathbf{p}}} \delta(p_0 - E_{\mathbf{p}}) \theta(k_F - |\mathbf{p}|) . \quad (\text{A2})$$

The polarization $\Pi_{\mu\nu}^j(q)$ involves only axial-vector vertex and is given by

$$\Pi_{\mu\nu}^j(q) = -i C^j(q^2) \int \frac{d^4 p}{(2\pi)^4} \text{Tr} \left[\Gamma_{\mu\beta} S^{\beta\alpha}(p') \Gamma_{\alpha\nu} G^o(p) \right] + (q_\alpha \rightarrow -q_\alpha) , \quad (\text{A3})$$

where $\Gamma_{\alpha\nu} = g_{\alpha\nu} - \gamma_\alpha \gamma_\nu / 4$. The off-shell term ($\gamma_\alpha \gamma_\nu / 4$) insures that the axial vector vertex satisfies the relation $\gamma^\mu \Gamma_{\mu\nu} = 0$. The coefficient functions $C^j(q^2)$ are given as

$$\begin{cases} \frac{4f_{\pi N\Delta}}{3\sqrt{2}m_\pi} \cos\theta_c G_A(q^2) r_{N\Delta} & \text{for } j = \pi^\pm; \\ \frac{2f_{\pi N\Delta}}{3m_\pi} G_A(q^2) r_{N\Delta} & \text{for } j = \pi^0 . \end{cases} \quad (\text{A4})$$

Here θ_c is the Cabbibo angle and $G_A(q^2)$ is the axial-vector form factor for the p-h excitation. The value of the axial vector $N\Delta$ transition strength $r_{N\Delta}$ is somewhat model dependent and we choose an intermediate value 2 in our calculation.

After some algebra, Eq. (A3) becomes

$$\Pi_{\mu\nu}^j(q) = -C^j(q^2) \int_M^{E_F} dE_{\mathbf{p}} \int_{-1}^1 d\chi \frac{|\mathbf{p}|}{8\pi^2} \frac{T_{\mu\nu}}{(p+q)^2 - M_\Delta^2 + i\epsilon} + (q_\alpha \rightarrow -q_\alpha) . \quad (\text{A5})$$

Here $T_{\mu\nu}$ is the result of the Dirac trace,

$$\begin{aligned} T_{\mu\nu} &= \frac{1}{6M_\Delta^2} \left[3p_\mu p'_\nu p'^2 + 3p_\nu p'_\mu p'^2 + p \cdot p' g_{\mu\nu} p'^2 - 16p \cdot p' p'_\mu p'_\nu \right. \\ &\quad \left. - 3M_\Delta^2 (p_\mu p'_\nu + p_\nu p'_\mu - 5p \cdot p' g_{\mu\nu}) \right. \\ &\quad \left. + 2MM_\Delta (9g_{\mu\nu} M_\Delta^2 - g_{\mu\nu} p'^2 - 8p'_\mu p'_\nu) \right] , \end{aligned} \quad (\text{A6})$$

and E_F is the Fermi energy $E_F = \sqrt{k_F^2 + M^2}$, and the $\chi = \cos\theta$ is the angle between \mathbf{q} and \mathbf{p} . As long as Δ is stable, the angular integration can be done analytically while the remaining integration over $E_{\mathbf{p}}$ is performed numerically. A similar calculation in a mean field approximation can be done by replacing M and M_Δ by the effective masses. The

contribution from vector mean field is eliminated by a change of variable in the energy integration. We include the Δ decay width by replacing the Δ mass in the denominator of Eq. (A5) as

$$M_{\Delta} \rightarrow M_{\Delta}^c \equiv M_{\Delta} - i\Gamma/2 , \quad (\text{A7})$$

and the double integrations are done numerically.

REFERENCES

- [1] R. Becker-Szendy *et al.*, Phys. Rev. D **46**, 3720 (1992).
- [2] K. S. Hirata *et al.*, Phys. Lett. B **280**, 146 (1992); K. S. Hirata *et al.*, Phys. Lett. B **205**, 416 (1988); E. W. Beier *et al.*, Phys. Lett. B **283**, 446 (1992).
- [3] J. Engel, E. Kolbe, K. Langanke, and P. Vogel, Phys. Rev. D **48**, 3048 (1993).
- [4] GALLEX Collaboration, Phys. Lett. B **285**, 376 (1992) ; A. I. Abazov *et al.*, Phys. Rev. Lett. **67**, 3332 (1991); K. S. Hirata *et al.*, Phys. Rev. D **44**, 2241 (1991).
- [5] Masayuki Nakahata *et al.*, J. Phys. Soc. of Japan **55** 3786 (1986).
- [6] G. L. Fogli and G. Nardulli, Nucl. Phys. **B160**, 116 (1979).
- [7] Hungchong Kim, J. Piekarewicz and C.J. Horowitz, Phys. Rev. C **51**, 2739 (1995).
- [8] B. D. Serot and J. D. Walecka, in *Advances in Nuclear Physics*, edited by J.W. Negele and E. Vogt (Plenum, New York, 1986), Vol. 16.
- [9] Hungchong Kim, S. Schramm and C. J. Horowitz, To be published in Phys. Rev. C.
- [10] K. Wehrberger, C. Bedau and F.Beck, Nucl. Phys. **A504**, 797 (1991).
- [11] M. J. Dekker, P. J. Brussaard, and J. A. Tjon, Phys. Rev. C **49**, 2650 (1994).
- [12] P. Carruthers and Michael Martin Nieto, Ann. Phys. (N. Y.) **51**, 359 (1969).
- [13] I. S. Towner, Phys. Rep. **155**, 263 (1987).
- [14] C. J. Horowitz and B. D. Serot, Nucl. Phys. **A368**, 503 (1981).
- [15] K. Wehrberger and R. Wittman, Nucl. Phys. **A513**, 603 (1990).
- [16] T. Hennino *et al.*, Phys. Lett. B **283**, 42 (1992); J. Chiba *et al.*, Phys. Rev. Lett. **67**, 1982 (1991).
- [17] B. K. Jain, J. T. Londergan and G. E. Walker, Phys. Rev. C **37**, 1564 (1988).
- [18] E. J. Moniz and Alpar Sevgen, Phys. Rev. C **24**, 224 (1981).
- [19] Y. Fukuda *et al.*, Phys. Lett. **B335**, 237 (1994).

FIGURES

FIG. 1. Feynman diagram for coherent pion production through Δ -h excitations. In the charged-current reaction, k' is the four momentum of the muon or electron, and q is the momentum of the W^\pm boson. In the neutral-current reaction, k' is the momentum of the scattered neutrino and q the momentum of the exchanged Z^0 .

FIG. 2. Differential cross section $d\sigma/dE_{k'}$ as a function of muon energy $E_{k'}$. The thick solid and dashed curves are for the free Δ -h calculations, without and with decay width, respectively. The thick dot-dashed curve is the free p-h calculation. The corresponding thin curves are for MFA. The short dashed curve is the RPA p-h calculation.

FIG. 3. (a) shows events per kiloton-year versus muon energy. The bold solid line represents the free Δ -h calculation with decay width 115 MeV, and the bold dashed line is for Δ -h in MFA. The thin lines are the corresponding p-h results. Events calculated in RPA are given by the dot-dashed curve. In figure (b), the solid curve is the ratio of mean field to free Fermi gas calculations for p-h excitations and the dashed curve is the similar ratio of Δ -h events. The dots give the ratio of RPA to free p-h and the dot-dashed curve is the ratio of free Δ -h over an RPA calculation of p-h yields.

FIG. 4. (a) shows electron events calculated in the Fermi gas model (short-dashed curve) and RPA (dot-dashed) involving only p-h excitations versus electron energy. Also shown are the coherent π^0 events calculated for Δ 's with (bold long-dashed) and without decay width (bold solid). The corresponding thin curves are the cases including mean fields. (b) shows the similar curves for coherent charged pions. In this case, the events are plotted versus visible energy as discussed in the text.

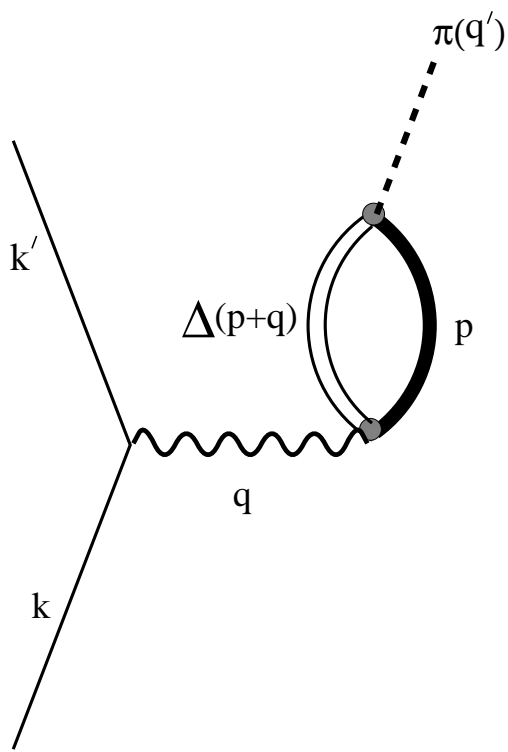


Figure 1

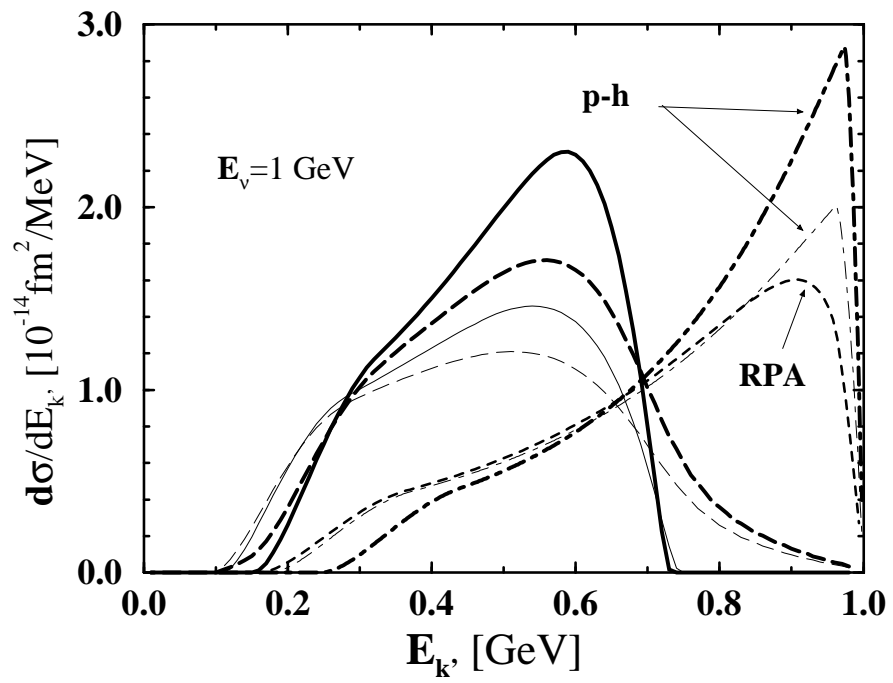


Figure 2

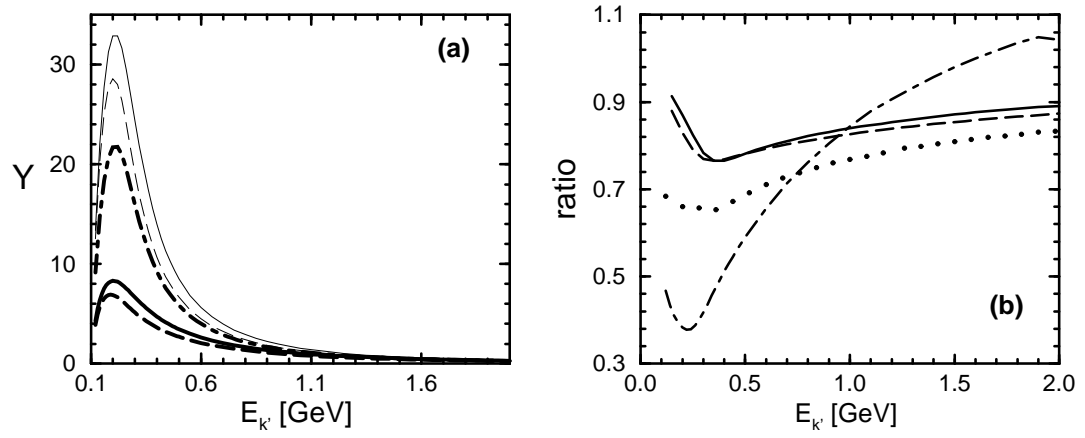


Figure 3

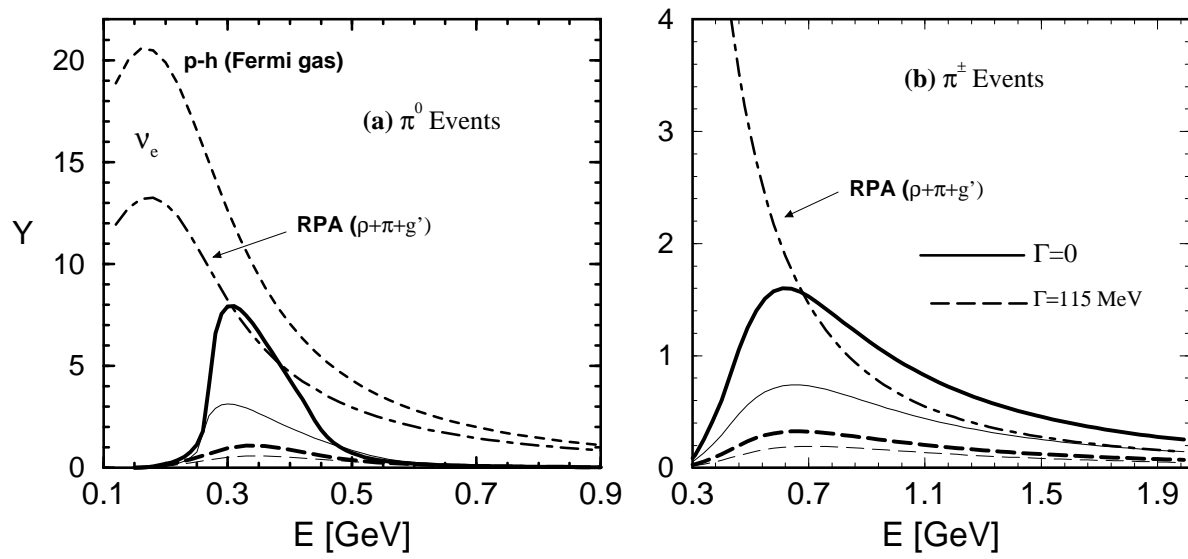


Figure 4